NASA TECHNICAL MEMORANDUM

NASA TM X-52442

ATTENUATION OF SOUND IN SOFT WALLED CIRCULAR DUCTS

by Edward J. Rice
Lewis Research Center
Cleveland, Ohio

TECHNICAL PAPER proposed for presentation at Symposium on Aerodynamic Noise sponsored by the Air Force Office of Scientific Research and the University of Toronto Institute for Aerospace studies
Toronto, Canada, May 20-21, 1968

NATIONAL AERONAUTICS AND SPACE ADMINISTRATION · WASHINGTON, D.C. · 1968

ATTENUATION OF SOUND IN SOFT WALLED CIRCULAR DUCTS

by Edward J. Rice

Lewis Research Center
Cleveland, Ohio

TECHNICAL PAPER proposed for presentation at

Symposium on Aerodynamic Noise
sponsored by the Air Force Office of Scientific Research and
the University of Toronto Institute for Aerospace Studies
Toronto, Canada, May 20-21, 1968

NATIONAL AERONAUTICS AND SPACE ADMINISTRATION

ATTENUATION OF SOUND IN SOFT WALLED CIRCULAR DUCTS

Edward J. Rice
Lewis Research Center
National Aeronautics and Space Administration
Cleveland, Ohio

E-4464

SUMMARY

A theory is presented which appears capable of predicting the attenuation of broad-band sound in soft walled (low acoustical impedance) circular ducts.

The axially symmetric separable solutions to the linear wave equation in clyindrical coordinates were obtained. It was assumed that the steady velocities and pressure fluctuations were small. The first ten characteristic function solutions were fit to form a traveling plane pressure wave at the lined duct entrance by means of a Fourier-Bessel series expansion. The eigenvalues are complex numbers due to the finite wall impedance boundary condition.

The present theory, in contrast to the approximate theory valid for hard walls, shows a strong dependence of sound attenuation on frequency. This dependence occurs through the ratio of the duct diameter to sound wavelength.

At high frequencies focusing of the sound wave toward the duct axis occurs. The acoustic energy can remain high, but at the outside wall, where the energy must be absorbed, the pressure oscillations may be small.

The theory was used to calculate the noise reduction obtained with a perforated plate liner on a J-65 engine inlet. The liner design was based upon an approximate theory valid for very hard walls. The present theory showed excellent agreement with experimental measurements and why the design based on approximate theory failed to provide high noise reduction.

SYMBOLS

A	area, ft^2
B_j	constant (see eq. (5) and (13))
C	speed of sound, ft/sec
C_p	specific heat at constant pressure, $Btu/lb_m/^oR$
D	duct diameter, ft
D/λ	duct diameter to wavelength ratio (see η below)
dB_{max}	maximum possible sound power attenuation for a given η and L/D, decibels
E	acoustic energy, ft lb_f/sec

E_{jk}	acoustic energy contribution of j pressure and k axial velocity modes, ft lb_f/sec
f	sound frequency, Hz
J_n	Bessel function of the first kind, of order n
L/D	duct length to diameter ratio
L	duct length, ft
P_j	j mode of acoustic pressure, psi
P*	complex conjugate of P, psi
P	acoustic pressure, $\sum_j P_j$, psi
R_j	modulus of j complex eigenvalue
$\mathfrak{R}$	gas constant, ft $lb_f/lb_m/^oR$
r	radial space coordinate, ft
r_w	duct radius, ft
T	temperature, ^oR
t	time, sec
v	acoustic velocity, $\sum_j v_j$, ft/sec
v_j	j mode of acoustic velocity, ft/sec
X	axial space coordinate, ft
Z	liner acoustic impedance, $lb_m/ft^2/sec$
α_j	complex eigenvalue of j radial characteristic solution ($\alpha_j = R_j e^{i\theta j}$)
ζ	dimensionless liner acoustical impedance ($Z/\rho_o C$)
η	Morse's frequency parameter, duct diameter in wavelengths $r_w\omega/\pi C$ or D/λ
θ_j	argument of j complex eigenvalue
λ	sound wavelength, ft
ρ	density, lb_m/ft^3
ρ_o	average density, lb_m/ft^3

σ_j, τ_j Morse's transmission parameters (ref. 2)

Φ dimensionless acoustical resistance, $\mathfrak{Re}(\zeta)$

χ dimensionless acoustical reactance, $\mathfrak{Im}(\zeta)$

ω circular frequency, rad/sec

$(\ )^*$ complex conjugate

1. INTRODUCTION

The solution to the linearized acoustical wave equation in circular ducts is well known and the method of applying boundary conditions to the characteristic solutions to represent a complicated waveform entering a soft walled duct is thoroughly established, (refs. 1 and 2). Due to computational difficulties, an approximate solution to the duct wall impedance equation for the first mode of vibration has been made in the past, (refs. 1, 3, and 4). The resulting solution is an approximation to the transmission of a plane wave in a circular duct with a nearly hard wall.

The purpose of this paper is to investigate the complete solution of the linearized wave equation with associated boundary conditions such that the solution is valid for ducts with very soft walls (i.e., acoustically lined ducts). The solution is specialized to that of a plane wave entering the duct but could be applied to any axisymmetric wave form.

The theory was applied to broad-band or random noise in the following way. At each frequency in the broad-band spectrum the random noise was assumed to enter the duct as a plane traveling pressure wave. The attenuation of this pressure wave was calculated at each frequency and compared to that obtained experimentally in the inlet of a J-65 turbojet engine. The comparison between experimental and theoretical sound power attenuation was excellent.

2. THEORY

Differential Equation and Solutions. The equations of motion for the air in the duct are:

$$\left.\begin{aligned} \frac{\partial \rho}{\partial t} &= -\nabla \cdot (\rho v) && \text{cont.} \\ \rho \frac{Dv}{Dt} &= -\nabla p && \text{mom.} \\ \rho C_p \frac{DT}{Dt} &= \frac{Dp}{Dt} && \text{energy} \\ p &= \rho \mathfrak{R} T && \text{state} \end{aligned}\right\} \qquad (1)$$

Viscous and heat transfer terms have been neglected. The air in the duct is assumed to behave as an ideal gas. If it is assumed that the pressure perturbations are small compared to the average

pressure and the steady velocities are negligible, equation (1) reduces to:

$$\left.\begin{aligned} \frac{\partial p}{\partial t} &= -\rho_o C^2 \nabla \cdot v \\ \rho_o \frac{\partial v}{\partial t} &= -\nabla p \end{aligned}\right\} \tag{2}$$

Equations (2) can be combined to obtain the wave equation,

$$\nabla^2 p = \frac{1}{C^2} \frac{\partial^2 p}{\partial t^2} \tag{3}$$

and if the time dependence in pressure is of the form $e^{i\omega t}$ then

$$v = \frac{i}{\rho_o \omega} \nabla p \tag{4}$$

The solution of equation (3) in cylindrical coordinates with axial symmetry is:

$$P_j = B_j J_o\left(\alpha_j \frac{r}{r_w}\right) \exp\left[i\omega t - \frac{\omega}{C}(\sigma_j + i\tau_j)X\right] \tag{5}$$

The subscript j is used in equation (5) since there are an infinite number of solutions of this form.

The radial eigenvalues α_j must be determined from the boundary condition at the wall $(r = r_w)$ and can be expressed as:

$$\alpha_j = R_j e^{i\theta_j} \tag{6}$$

The constants B_j must be determined from the initial pressure wave at the duct entrance $(X = 0)$.

It should be noted that the argument of the Bessel function and thus the Bessel function itself is a complex number. The methods used for calculation of the complex Bessel function are presented in the appendix.

Application of Boundary Conditions. Each solution (eq. (5)) must satisfy the radial impedance condition at the outer wall:

$$Z = \left(\frac{P_j}{v_{rj}}\right)_{r=r_w} \tag{7}$$

Equation (4) is used to obtain the radial velocity (v_{rj}). Equation (7) can then be expressed as:

$$\frac{Z}{\rho_o C \eta} = \frac{\zeta}{\eta} = \frac{i\pi J_o(\alpha_j)}{\alpha_j J_1(\alpha_j)} \tag{8}$$

where

$$\eta = \frac{D}{\lambda} = \frac{2r_w f}{C} \tag{9}$$

The radial eigenvalues α_j must be determined from equation (8) and are a function of ζ/η only. The methods used to determine the α_j are presented in the appendix.

Since the differential equation in pressure (eq. (3)) is linear, the pressure can be expressed as the summation of individual solutions. The pressure in the lined duct can then be expressed in a Fourier-Bessel series of solutions of the form of equation (5):

$$P = \sum_j P_j = \exp(i\omega t) \sum_j B_j J_o\left(\alpha_j \frac{r}{r_w}\right) \exp\left[-\frac{\omega}{C}(\sigma_j \pm i\tau_j)X\right] \tag{10}$$

For an initial plane traveling pressure wave the pressure must be:

$$P = \exp(i\omega t), \qquad (X = 0) \tag{11}$$

Combining equations (10) and (11), the following equation for the constants B_j results:

$$\sum_j B_j J_o\left(\alpha_j \frac{r}{r_w}\right) = 1 \tag{12}$$

The radial characteristic functions form an orthogonal set between $r = 0$ and $r = r_w$ (ref. 5). The B_j can thus be determined in equation (12), and the result is:

$$B_j = \frac{i2\zeta}{\pi\eta\left[\left(\frac{\zeta\alpha_j}{\pi\eta}\right)^2 - 1\right]J_o(\alpha_j)} \tag{13}$$

With equation (13) substituted in equation (10), the pressure anywhere in the lined duct is determined.

The complete solutions for the pressure and radial velocity also satisfy the radial impedance boundary conditions since:

$$\frac{P}{v_r} = \frac{\sum_j P_j}{\sum_j v_{rj}} = \frac{\sum_j Z v_{rj}}{\sum_j v_{rj}} = Z \tag{14}$$

Axial Acoustic Energy. The axial intensity can be expressed as (ref. 6):

$$I = 1/2 \quad \mathrm{Re} \quad (P^* v_x) \tag{15}$$

Axial acoustic energy can thus be determined from:

$$E = \sum_{j,k} E_{jk} \tag{16a}$$

where

$$E_{jk} = \int I_{jk} \, dA = \pi \left[\mathrm{Re} \left(\int_0^{r_w} r P_j^* v_{xk} \, dr \right) \right] \tag{16b}$$

The subscripts jk signify the interaction of the j pressure mode with the k axial velocity mode. Equation (16a) must be used since:

$$E_{jk} \neq 0 \qquad (j \neq k) \tag{17}$$

In the evaluation of the integral of equation (16b)

$$\int_0^{r_w} r J_o\left(\alpha_j^* \frac{r}{r_w}\right) J_o\left(\alpha_k \frac{r}{r_w}\right) dr$$

$$= \frac{i\pi\eta r_w^2 (\zeta + \zeta^*) J_o(\alpha_j^*) J_o(\alpha_k)}{\zeta\zeta^* (\alpha_k^2 - \alpha_j^{*2})} \tag{18}$$

was used.

Equation (18) was derived from the equation for the "Orthogonality of Characteristics Functions" given in reference 5. Equation (8) and

$$\left[J_o(\alpha_j)\right]^* = J_o(\alpha_j^*) \tag{19}$$

were also used in the derivation of equation (18).

Equations (4), (5), (8), (13), (16b), and (18) yield:

$$E_{jk} = \frac{4 r_w^2}{\rho_o c \eta} \quad \mathrm{Re} \left[\frac{(\sigma_k + i\tau_k)(\zeta + \zeta^*) \exp\left\{ -\frac{\omega}{c} \left[(\sigma_j + \sigma_k) + i(\tau_k - \tau_j) \right] X \right\}}{Q_j^* Q_k (\alpha_k^2 - \alpha_j^{*2})} \right] \tag{20}$$

where

$$Q_k = \left(\frac{\zeta\alpha_k}{\pi\eta}\right)^2 - 1 \tag{21}$$

and Q_j^* is determined from equation (21) by replacing k by j and taking the complex conjugate.

The damping and transmission parameters can be determined by substituting equation (5) into equation (3). The real and imaginary parts of the resulting equation can be solved for σ_j and τ_j. The result is:

$$\sigma_j;\tau_j = \frac{1}{\sqrt{2}}\left\{\pm\left[\left(\frac{R_j}{\pi\eta}\right)^2\cos 2\theta_j - 1\right] + \left[\left(\frac{R_j}{\pi\eta}\right)^4 - 2\left(\frac{R_j}{\pi\eta}\right)^2\cos 2\theta_j + 1\right]^{1/2}\right\}^{1/2} \tag{22}$$

where (+) is used for σ_j and (-) for τ_j. From equation (6) it is seen that R_j and θ_j are the modulus and argumentof the complex eigenvalue α_j.

The sound power attenuation can be calculated from

$$dB = 10\ \log_{10}\left(\frac{E_{exit}}{E_{entrance}}\right) \tag{23}$$

where E_{exit} and $E_{entrance}$ are calculated from equation (16a) using equations (20), (21), and (22). Before equations (20), (21), and (22) can be evaluated, the complex eigenvalues α_j must be calculated from the multiple solutions of equation (8). The method used to evaluate the α_j is outlined in the appendix.

From equation (8) the radial eigenvalues α_j are seen to be a function only of ζ/η. Equation (13) shows the B_j to be a function of ζ/η and α_j or thus only of ζ/η. The modal content of the plane pressure wave at the lined duct entrance (X = 0) is thus a function only of ζ/η according to equation (5). The damping and transmission parameters σ_j and τ_j are seen to be a function of ζ/η through R_j and θ_j. But, in addition, σ_j and τ_j contain η without ζ explicitly. The exponential of equation (20) contains the term expressible as:

$$\left(\frac{\omega X}{C}\right)_{X=L} = \frac{\omega L}{C} = 2\pi\eta\left(\frac{L}{D}\right) \tag{24}$$

where L is the length of lined duct and D is the diameter.

The variables on which the sound attenuation depends are thus ζ/η, η, and L/D or alternately ζ, η, and L/D.

Several pressure and velocity modes must be considered for soft walled ducts. The attenuation equation (eq. (23)) thus contains the Logarithm of the ratio of two complicated summations. Due to this complication no simplifying truncation of the theory yielding a simple

equation for attenuation has been obtained.

3. RESULTS AND DISCUSSION

The numerical results which follow were calculated on an IBM 7094 computer. The first ten radial modes were used.

Attenuation Contours and Maximum Attenuation. The sound power attenuation depends upon four variables: the wall resistance and reactance, the duct diameter to wave length ratio (η), and the duct length to diameter ratio (L/D). Figure 1 presents constant attenuation contours as a function of wall resistance and reactance. The other variables are fixed at $\eta = 1$ and $L/D = 3$. Also plotted in figure 1 are the results of reference 1 which can be expressed as:

$$dB = -17.36(L/D)\frac{\Phi}{(\Phi^2 + \chi^2)} \tag{25}$$

The following differences between the approximate theory of reference 1 and the more complete theory of this paper can be noted.

For a given wall resistance maximum attenuation occurs at negative wall reactance rather than at the wall tune point ($\chi = 0$).

The present theory predicts an absolute maximum sound attenuation at fixed values of η and L/D. Decreasing resistance ultimately reduces attenuation for any value of reactance. The approximate theory predicts local maxima, but for $\chi = 0$ the attenuation can be increased indefinitely by reducing resistance. The present theory agrees with the approximate theory for large wall impedance (ζ/η).

It should be noted that figure 1 is not a general attenuation plot which can be used for liner design. Figure 1 is valid only for a duct diameter to wavelength ratio (η) of one and $L/D = 3$. For other η and L/D the impedance for maximum attenuation will move in the impedance plane, and the peak attenuation will change.

Figure 2 presents the value of the absolute maximum sound attenuation as a function of duct diameter in wavelengths (η). Several curves of constant L/D are shown. The maximum attenuation ($-dB_{max}$) has been normalized by dividing it by the value of L/D for each curve. The following should be noted from figure 2. For very small η ($\eta \approx 0.1$) the maximum attenuation is weakly dependent upon η. Near $\eta = 1$ the maximum attenuation falls rapidly with increasing $\eta(\alpha\ 1/\eta^2)$. For large η maximum attenuation is approximately inversely proportional to η.

For $\eta > 1$ the maximum attenuation is approximately proportional to L/D. An extrapolation of the larger L/D curves to $\eta < 1$ indicates that for small η the attenuation per unit L/D decreases with L/D.

The locus of the maximum sound attenuation in the wall impedance plane is shown in figure 3. Several lines of constant η and L/D are presented. In general the locus for constant L/D shows that for increasing η (or f) the impedance for maximum attenuation moves to larger wall resistance and more negative reactance. The exception

is the inflection found in each constant L/D curve. The advent of this inflection occurs at roughly $\eta = L/D$.

The resistance of typical lining materials increases with frequency (see fig. 7). Unfortunately the reactance also increases with frequency. This trend of reactance with frequency is inverse to that required for maximum attenuation. Large sound attenuation can thus be obtained only over a limited frequency range for a given wall treatment.

Sound Power Attenuation Contour Breadth in Wall Impedance Plane. Structural considerations may preclude the use of a liner material with optimum wall impedance. The question then arises. How far removed from the optimum wall impedance can the liner impedance be and still result in acceptable sound attenuation? Figures 4 and 5 are presented to partially answer this question.

Figure 4(a) represents vertical cuts through the maximum attenuation points of several contour plots like figure 1. Figure 4(a), for an $L/D = 1$, was constructed in the following way. For a fixed diameter to wavelength ratio (η) and for the wall reactance of maximum attenuation, sound attenuations for several resistances on both sides of the maximum attenuation were calculated. Plots of attenuation versus resistance were made. These plots provided the resistances for say 5, 10, 20, etc. dB sound attenuations. These resistances were then plotted on figure 4(a) for the value of η used. A range of η was covered with the unique value of reactance for each η which provides maximum attenuation. Figure 4(b) was generated like figure 4(a) but with the roles of resistance and reactance interchanged. Figure 4(b) thus represents horizontal cuts through the maximum attenuation points of several contour plots like figure 1. Figures 5(a) and (b) are analogous to 4(a) and (b) but with $L/D = 5$.

The effect of L/D on the breadth of the sound attenuation contours is clear from figures 4 and 5, but numerical examples will further illustrate the effect. At the largest value of η for which 20 dB reduction can be obtained ($\eta = 1.13$ for $L/D = 1$ and $\eta = 3.85$ for $L/D = 5$) the breadth of the 10 dB contours were observed. For $L/D = 1$ the intervals are $0.2 \leq \Phi \leq 1.6$ and $-1.41 \leq X \leq -0.15$. For $L/D = 5$ they are $1.28 \leq \Phi \leq 8.9$ and $-6.5 \leq X \leq +0.5$. The breadth increases (due to an increase in L/D by a factor of 5) are thus 5.4 for resistance and 5.6 for reactance. The contour breadth is thus seen to increase approximately as L/D.

The benefits possible from using lined partitions in the duct are now obvious. Increasing L/D by a factor of 5 reduces η by a factor of 5 for the same L. Reducing η increases the maximum possible sound attenuation (fig. 2). An increase in L/D broadens the impedance range over which a given sound attenuation can be obtained. This is caused by the increased liner area as well as the reduction in η.

Beaming of Pressure Wave at High Frequency. Radial sound pressure profiles for $\eta = 0.1$, 1, and 10 for several values of L/D are shown in figure 6. The wall resistance and reactance were 1.6 and zero for all curves of figure 6.

At the lined duct entrance ($L/D = 0$) the pressure wave is a plane traveling wave of unit amplitude. This implies a uniform

amplitude and phase at any radius. At $L/D = 3$ the phase change from $r = 0$ to $0.9\ r_w$ is -4.6, -0.8, and +30.5 degrees for $\eta = 0.1$, 1, and 10 respectively. For large η the pressure near the wall is seen to lead that at the duct axis. From these phase relationships and the radial pressure profiles of figure 6 the following is apparent. For $\eta = 0.1$ and 1 the wave is attenuated and progresses down the duct as nearly a plane wave. For $\eta = 10$ the pressure wave is beamed toward the duct axis. For $L/D = 3$ and 5 the pressure oscillations at the duct axis are more than twice that of the original plane wave (at $L/D = 0$). At the duct wall the pressure oscillations have been reduced by a factor of about 10 (or 20 dB). The acoustic power has been redistributed toward the duct axis. At the wall where it must be absorbed, the sound intensity has been reduced. Thus, sound power attenuation is small as can be verified from the table of figure 6.

Comparison of Theory and Experimental Results. In order to calculate sound attenuation in a duct, the resistance and reactance of the lining material must be known. The resistance and reactance frequency dependence (calculated by method of ref. 7) used in the following calculations is presented in figure 7. Several resistance curves are shown since liner resistance varies with sound pressure level in the duct. The following data were used in the impedance calculations:

1. Steady flow velocity in duct, 350 fps.
2. Liner open area ratio, 0.08
3. Liner face plate thickness, 0.020 inches
4. Liner hole diameter, 0.050 inches
5. Liner back cavity depth, 1 inch

Also included in figure 7 are two extra scales (η_1 and η_5) relating $\eta(D/\lambda)$ to frequency for $L/D = 1$ and 5 where $L = 30$ inches.

Experimental sound power attenuation data was obtained with a lined inlet on a J-65 turbojet engine. The lined duct inside diameter (D) was 30 inches, and the lined length (L) was 30 inches (thus $L/D = 1$). The evaluation method of sound power levels is found in reference 9. The experimental sound power attenuation obtained with the lined inlet (properties as in figure 7) are shown by the data points in figure 8(b).

Sound power attenuations (using the present theory) were calculated for several sound pressure levels and a range of frequencies. The experimental apparatus dimensions were used. The results are shown in figure 8(a). The theoretical sound power attenuation is shown by the solid curve in figure 8(b). This curve was obtained by using the experimental sound pressure level at several frequencies and interpolating in figure 8(a). The agreement with experiment is seen to be excellent and within the experimental error (2dB).

The dashed line of figure 8(b) shows the low frequency end of the attenuation curve predicted by the approximate theory of reference 1 (see eq. (25) this paper). This curve continues rising with frequency and would predict about 18 dB sound power reduction at the linear tune point (4175 Hz). No reduction at this frequency was observed experimentally.

The reason for the failure of this lined duct design to provide high sound attenuation is seen in figures 4(a) and (b). The 130 dB level resistance and the reactance are plotted as dashed curves with frequencies noted on the curves. The liner resistance and reactance

diverge further from the region of high damping with increasing frequency. Above 1,000 hertz both resistance and reactance are in the low attenuation region.

An example of how a geometry change can effect sound attenuation is shown in figure 9. The same liner material as in figure 7 was used. The lined duct length remains at 30 inches, but L/D was changed to 5 (say by lined partitions). The theoretical sound attenuation was calculated for three sound pressure levels. High sound attenuation is seen to be possible over a wide frequency range. For comparison the 150 dB level sound attenuation curve of figure 8(a) has been replotted in figure 9. A change from $L/D = 1$ to 5 is seen to increase the frequency for maximum attenuation from 1000 to 2300 hertz and to increase the peak from 5.3 to 51 dB.

The 130 dB level resistance and the reactance from figure 7 are plotted on figure 5(a) and (b). A comparison with figure 4(a) and (b) shows how a change only in L/D from 1 to 5 has moved the high attenuation impedance region.

4. CONCLUDING REMARKS

Comments on Duct Partitioning. Circular ducts have been partioned by the addition of radial lined sections (struts) and circumferential lined sections (rings) to increase the liner area to duct area ratio. With the proper selection of struts and rings the smaller resulting tubes can be made nearly square. Morse's approximate solution (ref. 1) for rectangular cross sections shows that equation (25) is valid for a square duct with very hard walls if D is replaced by a side of the square. Thus, in the limit of very hard walls the sound attenuation in circular and square ducts is the same. For soft walls the analysis of this paper should give at least qualitatively correct results for square ducts.

Comments on Liner Resistance and Sound Power Level. As the initial plane pressure wave progresses down the duct it will be attenuated and possibly beamed toward the duct axis (for $D/\lambda > 1$). The sound pressure level at the liner and thus the liner resistance (fig. 7) decreases down the duct. This effect could be handled by a new determination for the B_j of equation (10) at several locations along the duct. After the sound pressure level at the liner has dropped say 2 dB the characteristic solutions could be refitted to the remaining pressure wave (not necessarily a plane wave). This new solution could be used for a distance and then the refitting be repeated until the end of the duct is reached.

Approximate solutions could also be divised. The extremes of the sound power level at the liner, for instance, could be used in an attempt to bracket the exact solution.

The initial (duct entrance) sound pressure level was used in obtaining the theoretical curve (solid curve) of figure 8(b).

5. CONCLUSIONS

A theory that describes the propagation and attenuation of an

initially plane traveling pressure wave in a circular duct with an acoustically soft wall has been presented. The first ten characteristic function solutions were used in a Fourier-Bessel series to fit the plane traveling wave at the lined duct entrance. The results of the analysis may be summarized as follows.

1. For a duct diameter to wavelength ratio greater than one the initial plane wave was found to beam toward the duct axis. This results in a redistribution of the sound power within the duct. The sound pressure level at the wall liner, where acoustic energy must be absorbed, can be greatly reduced, while the sound power level is affected only slightly.

2. The theoretical sound power attenuation was found to agree well with experimental data. The data was taken with a cylindrical duct, lined with a perforated plate material, mounted on the inlet of a J-65 engine. The experimental suppressor was designed on the basis of an approximate theory valid for hard walls. The results of the present analysis show the reason that the suppressor design failed to provide high noise reduction.

3. For a given duct length to diameter ratio and duct diameter to wave length ratio an absolute maximum sound power attenuation was found in the liner impedance plane. This maximum was always found to be at negative wall reactance. With increasing duct diameter to wavelength ratio the maximum attenuation point was found to move to larger liner resistance and more negative liner reactance. The maximum sound power attenuation was found to be nearly proportional to L/D and to have a strong frequency dependence through the ratio of duct diameter to wavelength.

4. The region in the wall impedance plane over which a given sound power attenuation can be obtained increases approximately in proportion to L/D.

6. APPENDIX

Calculation of the Bessel Function with Complex Argument. The calculation of the Bessel function with complex argument was done in a computer program subroutine. The following calculation methods were used.

If $R \leq 10$ or if $R \leq (1 + (2\theta/\pi))n$ the infinite series definition (ref. 5) of the Bessel function was used as:

$$\left.\begin{aligned} J_n(Re^{i\theta}) &= \sum_{k=0}^{\infty} \frac{(-1)^k \left(\frac{Re^{i\theta}}{2}\right)^{2k+n}}{k!(k+n)!} \\ \text{or} \\ J_n(Re^{i\theta}) &= \sum_{k=0}^{\infty} \frac{(-1)^k \left(\frac{R}{2}\right)^{2k+n}}{k!(k+n)!} \left[\cos(2k+n)\theta + i \sin(2k+n)\theta\right] \end{aligned}\right\} \quad (26)$$

If $R > 10$ and $R > (1 + (2\theta/\pi))n$, the following asymptotic expansion (ref. 5) was used:

$$J_n(Re^{i\theta}) \sim \sqrt{\frac{2}{\pi Re^{i\theta}}} \left\{ U_n(Re^{i\theta}) \cos\left[G_n(Re^{i\theta})\right] - V_n(Re^{i\theta}) \sin\left[G_n(Re^{i\theta})\right] \right\} \tag{27}$$

where

$$G_n(Re^{i\theta}) = Re^{i\theta} - \frac{\pi}{4} - \frac{n\pi}{2} \tag{28}$$

$$\left.\begin{aligned} U_n(Re^{i\theta}) &= 1 + \sum_{k=1}^{\infty} \frac{(-1)^k S_{4k-1}}{(2k)!(8Re^{i\theta})^{2k}} \\ V_n(Re^{i\theta}) &= \sum_{k=1}^{\infty} \frac{(-1)^{k-1} S_{4k-3}}{(2k-1)!(8Re^{i\theta})^{2k-1}} \end{aligned}\right\} \tag{29}$$

and

$$S_j = (4n^2 - 1^2)(4n^2 - 3^2)(4n^2 - 5^2) \ldots (4n^2 - j^2)$$

The series of equation (29) were terminated in two ways: when the modulus of the k^{th} term of $U_n(Re^{i\theta})$ exceeded the modulus of the k^{th} term of $V_n(Re^{i\theta})$, or when the modulus of the k^{th} term of either was less than 10^{-10}.

Rapid convergence occurs in equation (26) for $R \ll n$ and in equation (27) when $R \gg n$. Both equations (26) and (27) were tested over wide ranges of R, θ, and n. For large n the dividing line between the two methods is $R = (1 + (2\theta/\pi))n$. If $R < 10$, equation (26) converges more rapidly for any n.

Double precision arithmetic was used in all cases.

Calculation of Complex Eigenvalues. The complex eigenvalues must be determined from the solution of equation (8) (derived in the text and repeated here).

$$\frac{Z}{\rho_o C \eta} = \frac{\zeta}{\eta} = \frac{i\pi J_o(\alpha_j)}{\alpha_j J_1(\alpha_j)} \tag{8}$$

where again:

$$\alpha_j = R_j e^{i\theta_j} \tag{6}$$

The method of reference 4 was used in the solution of equation (8) for large wall impedance.

Let

$$F = \left(\frac{R_j e^{i\theta_j}}{2}\right) \tag{30}$$

and

$$\epsilon = \frac{i\pi\eta}{2\zeta}$$

Using equation (6), substituting equation (30) into equation (8), and then differentiating equation (8) with respect to ϵ, there results:

$$(F + \epsilon^2)\frac{dF}{d\epsilon} = F \tag{31}$$

Equation (31) is a first order nonlinear differential equation which can be solved for F in an infinite series solution in ϵ.

The boundary conditions which must be applied are:

at $\epsilon = 0$

$$\left.\begin{aligned} &\theta_j = 0 \qquad \text{(all } j\text{)} \\ &\text{and } R_j \text{ is the } J^{th} \text{ root of } J_1(R_j) = 0 \end{aligned}\right\} \tag{32}$$

or $R_j = 0$, 3.8317, 7.0156, etc. for $j = 1, 2, 3$, etc.

For small wall impedance let

$$\xi = \frac{1}{\epsilon} \tag{33}$$

Substitution of equation (33) into equation (31) yields:

$$(1 + \xi^2 F)\frac{dF}{d\xi} + F = 0 \tag{34}$$

The boundary conditions are:

$$\left.\begin{aligned} &\text{at } \xi = 0 \qquad \theta_j = 0 \qquad \text{(all } j\text{)} \\ &\text{and } R_j \text{ is the } J^{th} \text{ root of } J_0(R_j) = 0 \end{aligned}\right\} \tag{35}$$

or $R_j = 2.4048$, 5.5201, 8.6437, etc. for $j = 1, 2, 3$, etc.

For every mode there is a region in the impedance plane where the series solutions of both equation (31) and equation (34) diverge (at least on the computer using double precision arithmetic). This region is around the branch line. The branch line is defined here as the curve in the liner impedance plane $(\Phi/\eta, \chi/\eta)$ on which two solutions to equation (8) have the same R but different θ ($R_j = R_k$ but $\theta_j \neq \theta_k$). The critical values of R_j on the branch line are 3.1962, 6.3064, . . . or:

$$R_{j,crit} \approx j\pi \tag{36}$$

In this critical impedance region the method of reference 8, for solving nonlinear equations, was applied directly to equation (8).

REFERENCES

1. Morse, P. M. Vibration and Sound. McGraw-Hill Book Co., Inc. 1948 (2nd ed.).
2. Morse, P. M. The Transmission of Sound Inside Pipes. J. Acoust. Soc. Am. 11, 205 (1939).
3. Molloy, C. T. and Honigman, E. Attenuation of Sound in Lined Circular Ducts. J. Acoust. Soc. Am. 16, 267 (1945).
4. Fisher, E. Attenuation of Sound in Circular Ducts. J. Acoust. Soc. Am. 17, 121 (1945).
5. Hildebrand, F. B. Advanced Calculus for Engineers. Prentice-Hall, Inc. 1949.
6. Morfey, C. L. Rotating Pressure Patterns in Ducts - Their Generation and Transmission. J. Sound Vibration 1, 60 (1964).
7. Phillips, B. Effects of High-Wave Amplitude and Mean Flow on a Helmholtz Resonator. NASA TM X-1582, 1968.
8. Marquardt, D. W. An Algorithm for Least-Squares Estimation of Nonlinear Parameters. Soc. Ind. Appl. Math. 11, 431, (1963).
9. Smith, L. J., Acker L. W. and Feiler, C. E. Sound Measurements on a Full-Scale Jet-Engine Inlet-Noise-Suppressor Cowling. Proposed NASA TN.

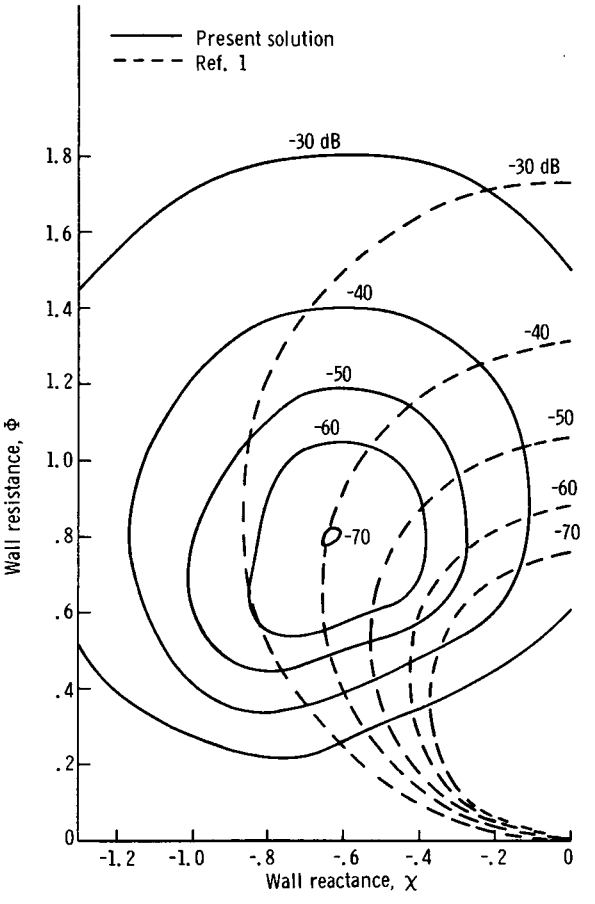

Figure 1. - Sound power attenuation contours for $\eta = 1$, L/D = 3.

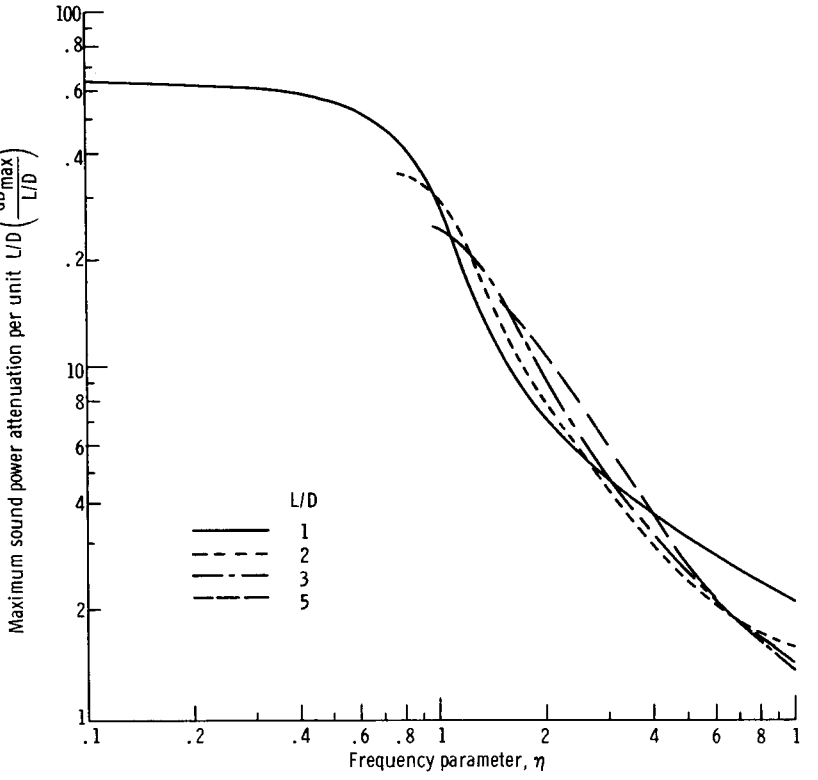

Figure 2. - Maximum possible sound power attenuation-frequency dependence.

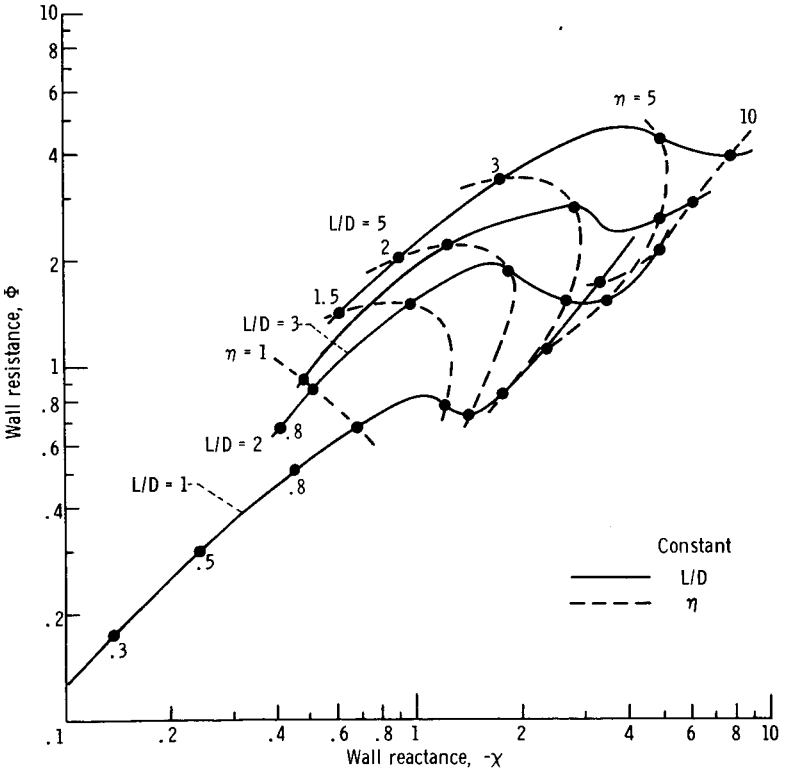

Figure 3. - Locus of maximum sound power attenuation in the wall impedance plane.

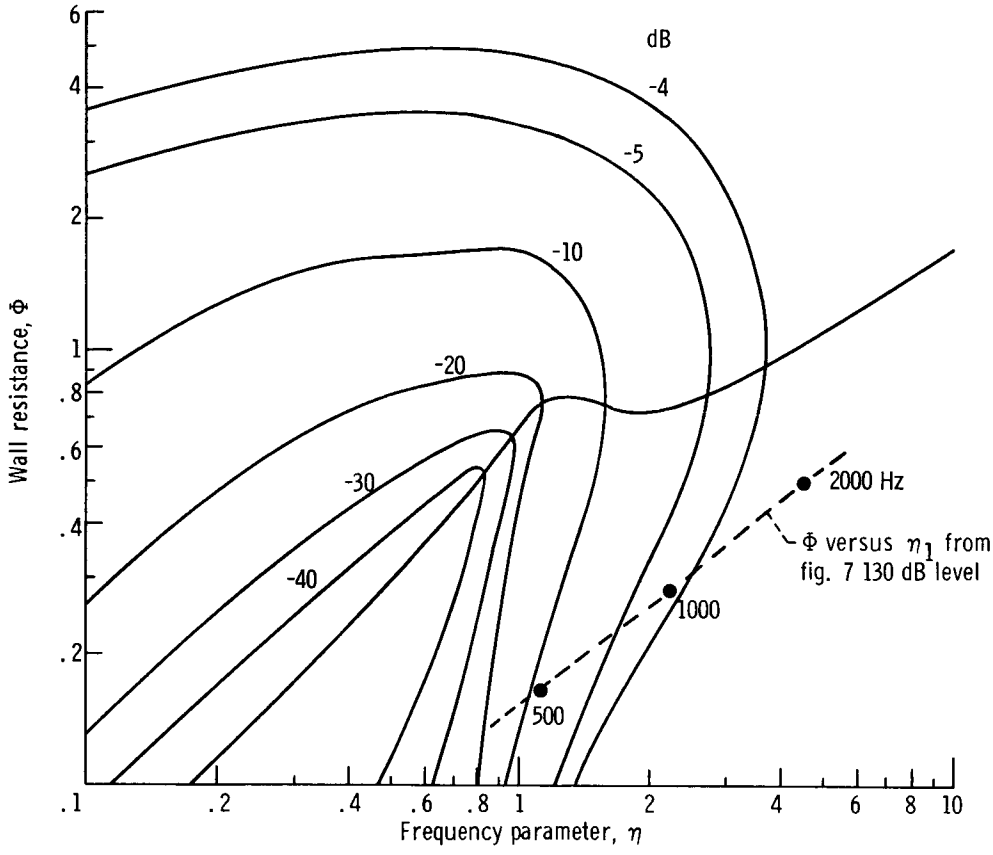

Figure 4(a). - Sound power attenuation contours at reactance of maximum attenuation (fig. 3) and L/D = 1.

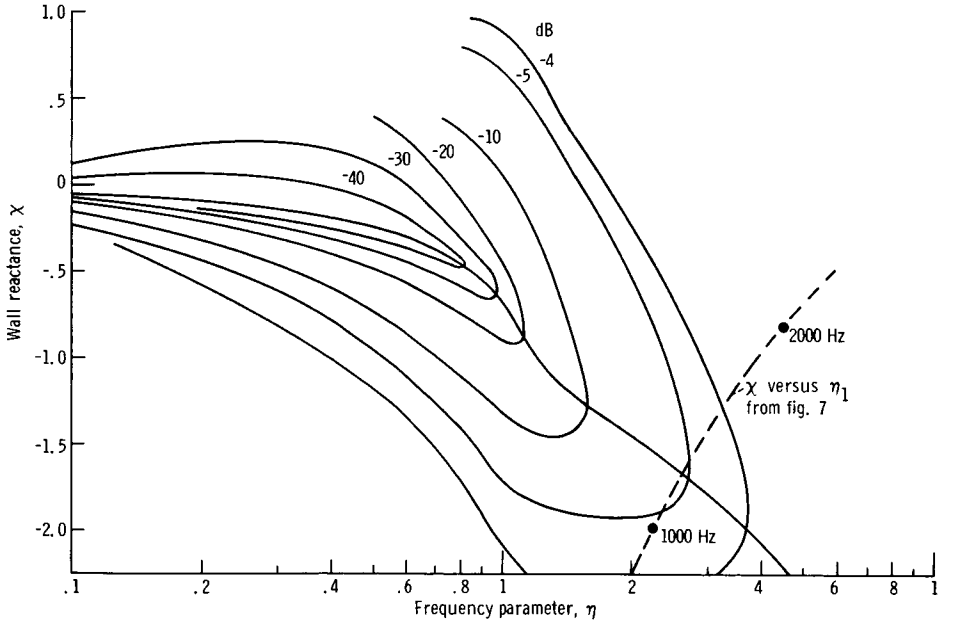

Figure 4(b). - Sound power attenuation contours at resistance of maximum attenuation (fig. 3) and L/D = 1.

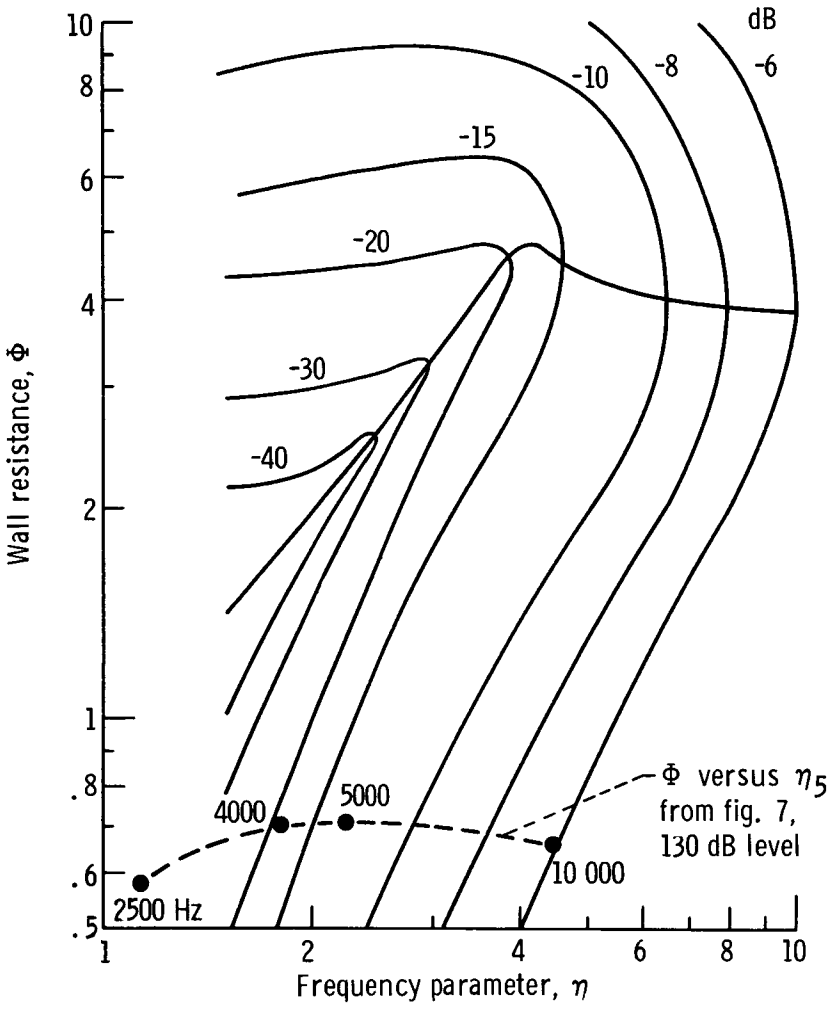

Figure 5(a). - Sound power attenuation contours at reactance of maximum attenuation (fig. 3) and L/D = 5.

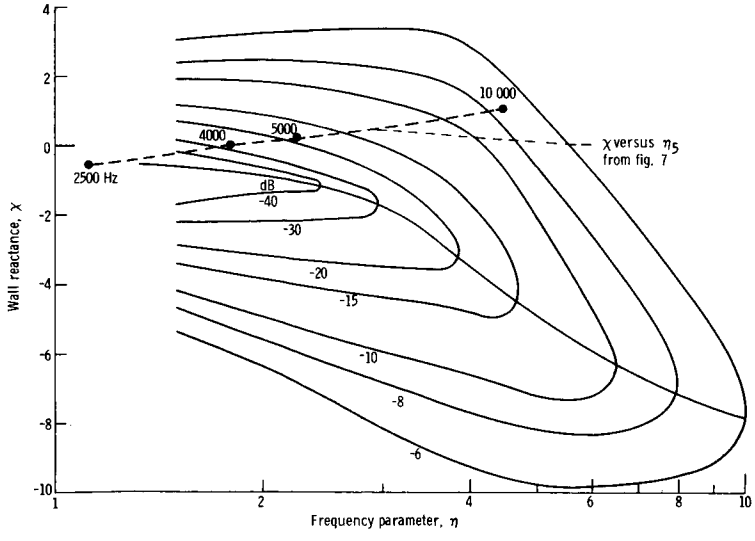

Figure 5(b). - Sound power attenuation contours at resistance of maximum attenuation (fig. 3) and L/D = 5.

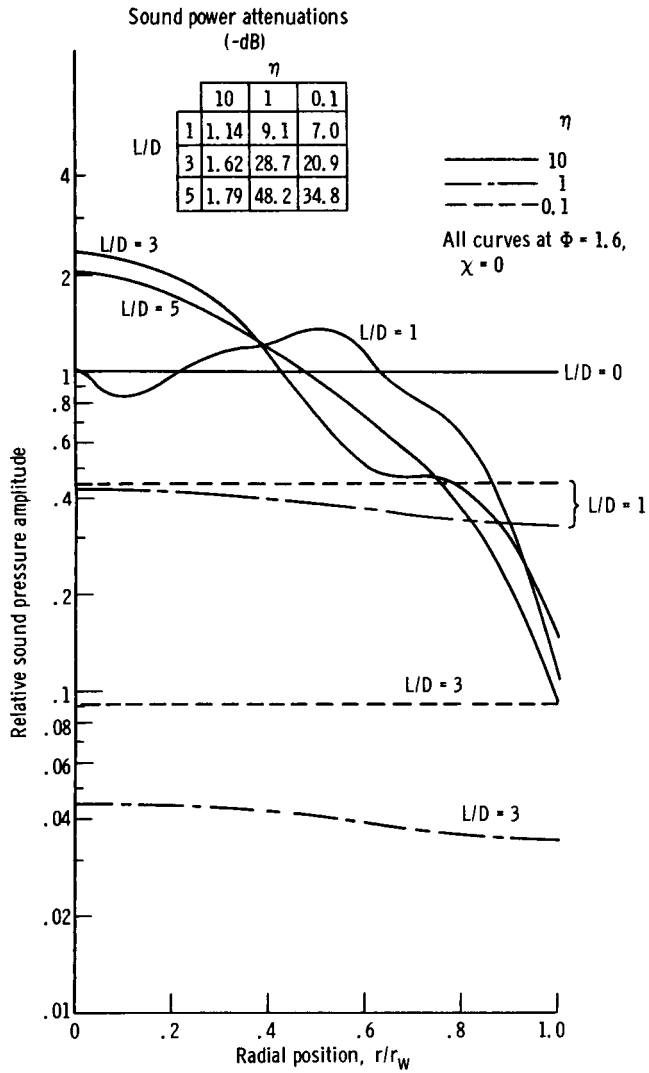

Figure 6. - Radial pressure profiles at several duct lengths.

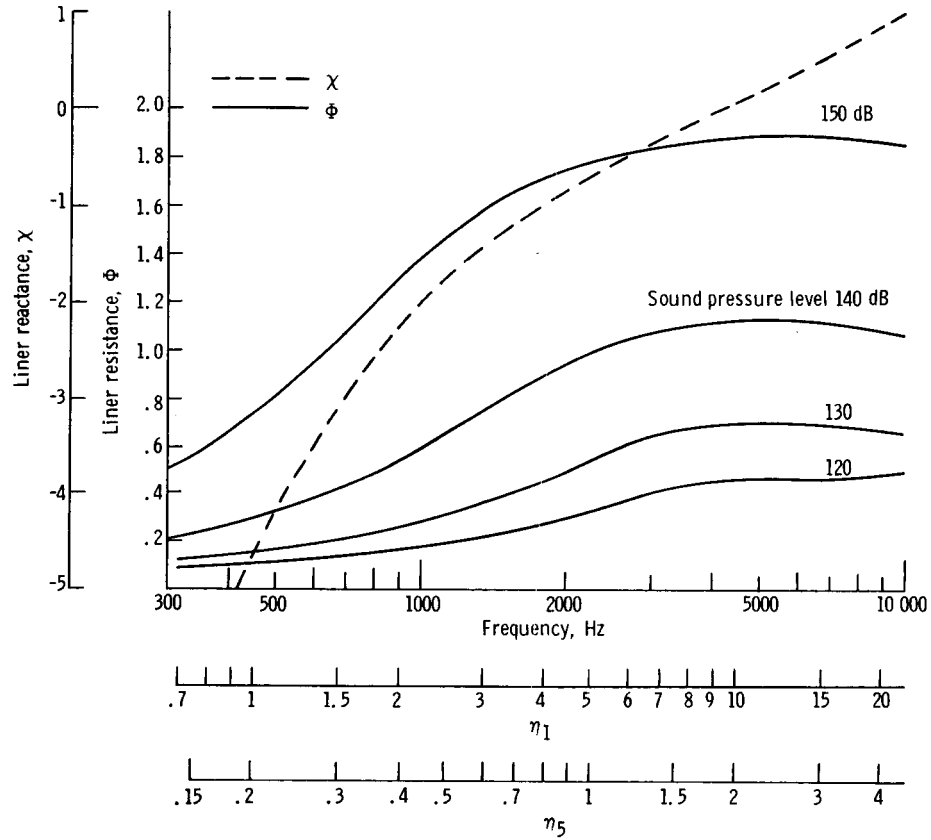

Figure 7. - Resistance and reactance of a perforated plate liner as a function of frequency. Calculations by method of reference 7. Steady flow-by velocity 350 fps, air 40° F. Liner open area ratio 0.08, thickness 0.02 inch, hole diameter 0.05 inch, back cavity depth 1 inch. η_1 and η_5 scales give η for L = 30 inches and L/D = 1 and 5.

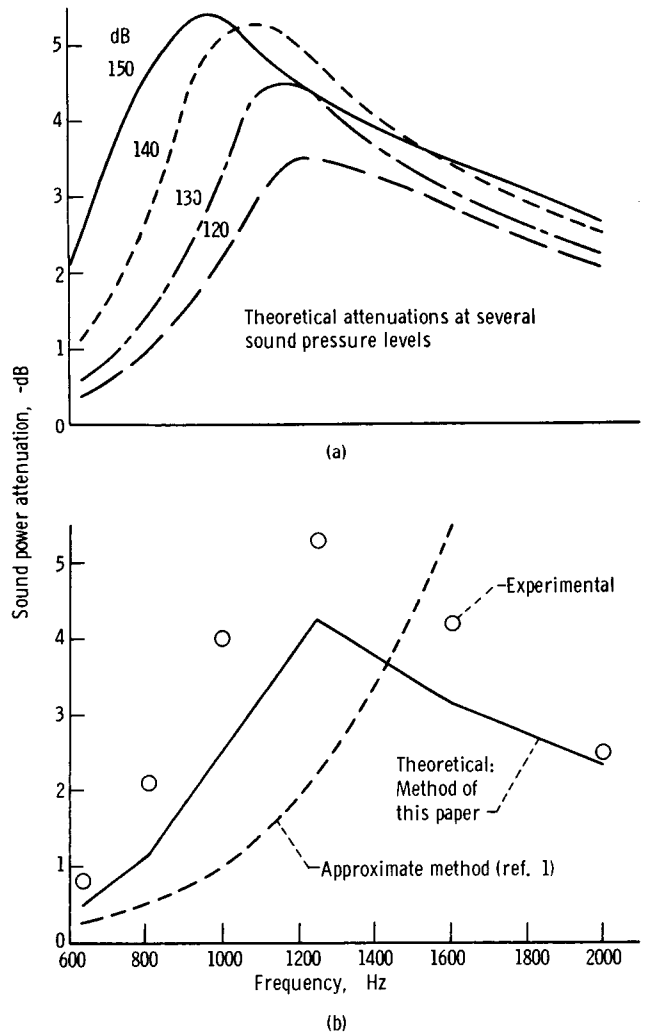

Figure 8. - Sound power attenuation frequency dependence, theoretical and experimental for L/D = 1 and L = 30 inches.

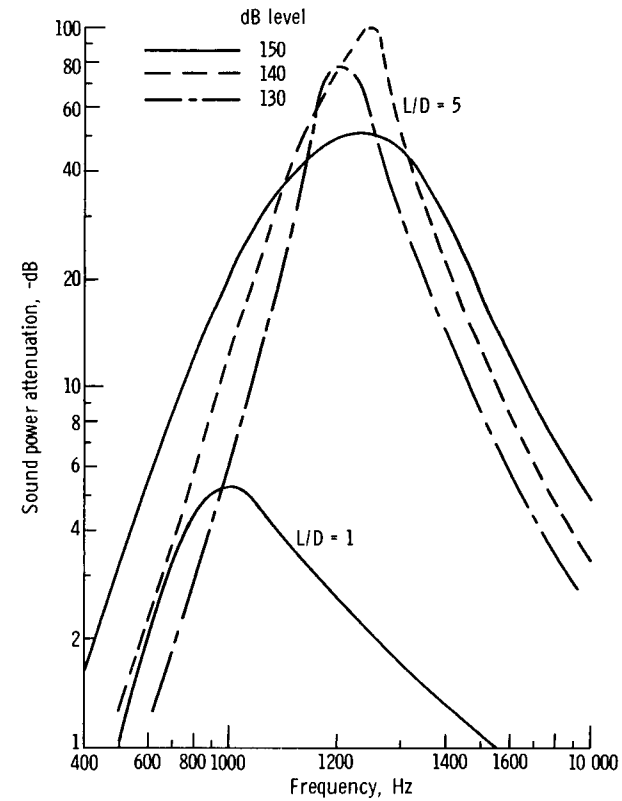

Figure 9. - Theoretical sound power attenuations for L/D = 1 and 5 with liner of figure 7 and L = 30 inches.

NASA-CLEVELAND, OHIO E-4464